

Free-surface cusps associated with flow at low Reynolds number

By JAE-TACK JEONG† AND H. K. MOFFATT

Department of Applied Mathematics and Theoretical Physics, University of Cambridge,
Silver Street, Cambridge, CB3 9EW, UK

(Received 7 August 1991)

When two cylinders are counter-rotated at low Reynolds number about parallel horizontal axes below the free surface of a viscous fluid, the rotation being such as to induce convergence of the flow on the free surface, then above a certain critical angular velocity Ω_c , the free surface dips downwards and a cusp forms. This paper provides an analysis of the flow in the neighbourhood of the cusp, via an idealized problem which is solved completely: the cylinders are represented by a vortex dipole and the solution is obtained by complex variable techniques. Surface tension effects are included, but gravity is neglected. The solution is analytic for finite capillary number \mathcal{C} , but the radius of curvature on the line of symmetry on the free surface is proportional to $\exp(-32\pi\mathcal{C})$ and is extremely small for $\mathcal{C} \gtrsim 0.25$, implying (in a real fluid) the formation of a cusp. The equation of the free surface is cubic in (x, y) with coefficients depending on \mathcal{C} , and with a cusp singularity when $\mathcal{C} = \infty$.

The influence of gravity is considered through a stability analysis of the free surface subjected to converging uniform strain, and a necessary condition for the development of a finite-amplitude disturbance of the free surface is obtained.

An experiment was carried out using the counter-rotating cylinders as described above, over a range of capillary numbers from zero to 60; the resulting photographs of a cross-section of the free surface are shown in figure 13. For $\Omega < \Omega_c$, a rounded crest forms in the neighbourhood of the central line of symmetry; for $\Omega > \Omega_c$, the downward-pointing cusp forms, and its structure shows good agreement with the foregoing theory.

1. Introduction

Some striking photographs of free-surface flows of both Newtonian and non-Newtonian fluids at low Reynolds numbers have been recently published in this *Journal* (Joseph *et al.* 1991, hereafter referred to as JNRR). These photographs provide compelling evidence for the formation of two-dimensional cusps on the free surface in regions of convergence of the flow to what would otherwise be a stagnation line. We have repeated the experiment of JNRR using a Newtonian fluid and a pair of counter-rotating cylinders, in the symmetric configuration of figure 1 (for experimental details, see §6). For very slow rotation rates, there is a stagnation line on the free surface, and in some circumstances a small rounded crest can form in the neighbourhood of this stagnation line (figure 1*a*). (This phenomenon was noted in an early investigation by Griggs (1939) in a paper concerned with the process of mountain formation by convection in the underlying lithosphere. Griggs carried out

† Present address: Department of Mechanical Engineering, Kum-Oh National Institute of Technology, 188 Shinpyung Dong, Kumi, Kyung Buk, Republic of Korea, 730-701.

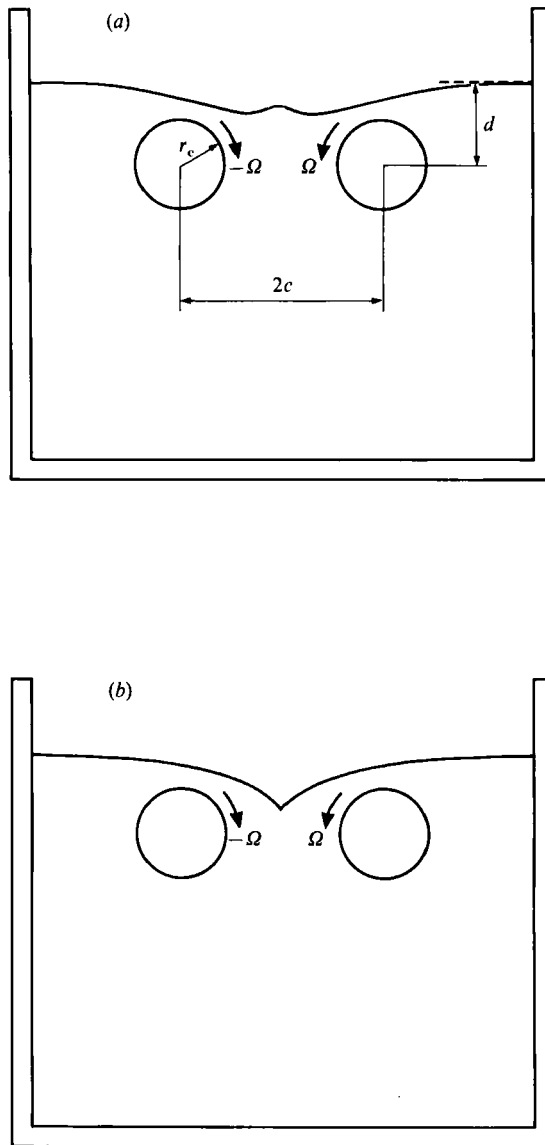


FIGURE 1. Experimental configuration showing the observed form of the free surface (a) when the rotation rate Ω is very small and (b) when Ω is larger. The range of Ω in the experiment was $0-7 \text{ s}^{-1}$. The fluid used was polybutene, and the range of Reynolds numbers $Re = \Omega r_c^2 / \nu$ was zero to 0.25; the range of capillary numbers \mathcal{C}_{exp} (see §6) was zero to 61.1, and of Froude numbers $Fr = \Omega(r_c/g)^{1/2}$ zero to 0.34. The ratio $\mathcal{C}_{\text{exp}}/Fr = \mu(r_c/g)^{1/2}/\gamma$ had the value 180.

a similar experiment to that described here, but with the cylinders rotated manually and with a layer of a mixture of heavy oil and sand on the fluid surface to simulate the Earth's crust.) When the rotation rate Ω is increased however, the surface dips downwards, and simple visual observation indicates the presence of a very sharp cusp on the free surface (figure 1b). If powder is sprinkled on the free surface, this powder is immediately swept through the cusp into the interior of the fluid. Thus, observation suggests that fluid particles on the free surface are similarly advected through the cusp into the interior.

There are, however, certain fundamental difficulties in accepting this conclusion,

convincing though the observational evidence may appear to be. First, a cusp is a singularity of curvature, and one would expect this singularity to be resolved by surface tension forces in its neighbourhood. JNRR proposed a solution in which the velocity is locally a small perturbation of a uniform stream U parallel to the (double) tangent at the cusp, the perturbation stream function being of the form $\psi = r^\lambda f(\theta)$, where λ is a parameter dependent on the capillary number $\mathcal{C} = \mu U/\gamma$ (where μ is viscosity, and γ surface tension). We comment in more detail on this solution in the following sections; for the moment it is sufficient to recall JNRR's conclusion that when $\mathcal{C} = \infty$, then $\lambda = \frac{3}{2}$, and the cusp has the local form $y \sim |x|^{\frac{2}{3}}$. The correct boundary conditions are then satisfied everywhere except at the singularity $x = 0$, $y = 0$ itself, which is in a sense where most of the interest of the problem resides! JNRR refer to an earlier discussion of cusp-type singularities by Richardson (1968) who proposed a local solution of the form

$$\psi = \frac{\gamma}{2\pi\mu} r \ln r \sin \theta, \quad (1.1)$$

(in plane polar coordinates) which is singular at $r = 0$, and is associated with a point force of magnitude 2γ exerted by the free surface on the fluid directed along the tangent at the cusp and out of the fluid. This solution suffers from the serious difficulties that the associated velocity is $O(\ln r)$ near $r = 0$, and the associated rate of dissipation of energy is infinite. Thus, although JNRR regard Richardson's solution as being valid in some extremely small neighbourhood of the cusp, this merely replaces one imperfection by another, and does nothing to resolve the real nature of the flow near the 'cusp' in a viscous fluid with non-zero surface tension.

There is a second major difficulty associated with the presence of the air outside the viscous liquid, which is subject to the no-slip condition at the free surface. If the cusp is genuine and fluid particles on the free surface do move into the interior of the fluid, then air must be entrained into the interior also. There is however no evidence in the experiments for the entrainment of air bubbles (although small bubbles can of course be deliberately injected to provide indicators of particle paths and rate of strain). This is a paradox reminiscent of that encountered in the famous moving contact-line problem (see, for example, Dussan V. & Davis 1974) in which strict application of the no-slip condition is in flat contradiction with both observation and common sense.

The object of the present paper is to provide a complete analytical solution of a model problem which does indeed reveal the full nature of the flow and the extent to which a description in terms of a cusp is legitimate. The model problem is an idealization of figure 1, in which the rotating cylinders are represented by a vortex dipole at fixed depth $d (= 1)$ below the undisturbed position of the free surface (figure 2*a*). The outer fluid boundaries are supposed moved to infinity, and we adopt the natural outer boundary condition $\mathbf{u} \rightarrow 0$ as $|\mathbf{x}| \rightarrow \infty$. The resulting problem is solved using complex analysis and conformal mapping techniques. The solution does confirm the formation of a cusp in the limit $\mathcal{C} \rightarrow \infty$. For finite \mathcal{C} however, the solution remains regular with a stagnation point on the free surface on the plane of symmetry. The radius of curvature R of the free surface at this stagnation point has the extraordinary behaviour

$$R/d \sim \frac{256}{3} \exp\{-32\pi\mathcal{C}\} \quad (1.2)$$

and is therefore extremely small when \mathcal{C} (defined by (2.24) below) is of order unity or greater. It is this behaviour that presumably leads to the extremely sharp cusp-like structures observed in experiments.

of curvature, taken positive if the centre of curvature is on the air side of the interface.

It is well-known that ψ can then be expressed in the form

$$\psi = \text{Im}(f(z) + \bar{z}g(z)), \quad (2.2)$$

where the overbar represents the complex conjugate, and $f(z)$, $g(z)$ are analytic functions at all points z in the fluid domain \mathcal{D} except at the singularity at $z = -i$ where

$$f(z) \sim \frac{i\alpha}{z+i} \quad (z \rightarrow -i). \quad (2.3)$$

The velocity components are then given by

$$u - iv = f'(z) + \bar{z}g'(z) - \overline{g(z)}, \quad (2.4)$$

and the pressure (p) and vorticity (ω) fields are given by

$$p - i\mu\omega = 4\mu g'(z). \quad (2.5)$$

It is easy to verify that, with these relations, the Stokes equation $\nabla p = \mu \nabla^2 \mathbf{u}$ is satisfied in the fluid. The condition $u, v \rightarrow 0$ as $|z| \rightarrow \infty$ are satisfied provided

$$f \sim cz, \quad g \sim \bar{c} \quad \text{as } |z| \rightarrow \infty, \quad (2.6)$$

where c is an arbitrary constant. We shall find that the choice $c = -i\gamma/4\mu$ is appropriate. The symmetry conditions $\psi = 0$, $\omega = 0$ on $x = 0$ clearly imply that

$$\text{Im}f(iy) = 0, \quad \text{Re}g(iy) = 0. \quad (2.7)$$

As shown by Richardson (1968), the boundary conditions on Γ take the form

$$f'(z) + \bar{z}g'(z) - \overline{g(z)} = u_0(z) \left(\frac{dz}{ds} \right), \quad (2.8)$$

$$f'(z) + \bar{z}g'(z) + \overline{g(z)} = -i \frac{\gamma}{2\mu} \left(\frac{dz}{ds} \right), \quad (2.9)$$

where s is the arclength on Γ measured from the point of symmetry B (figure 2*a*), and $u_0(z)$ is the (real) tangential velocity at an arbitrary point z of the free surface. Equation (2.9) is equivalent to (2.1). Manipulation of (2.8) and (2.9) yields the equations (for $z \in \Gamma$)

$$\text{Im} \left[\left(\frac{dz}{ds} \right) g(z) \right] = \frac{\gamma}{4\mu}, \quad (2.10)$$

and

$$f(z) + \bar{z}g(z) = 0. \quad (2.11)$$

Equations (2.3), (2.6) and (2.8)–(2.11) constitute the essential boundary conditions that $f(z)$ and $g(z)$ must satisfy.

Now let $z = w(\zeta)$ be the conformal mapping that maps the fluid domain \mathcal{D} to the unit disc $\mathcal{D}' : |\zeta| < 1$, and which places the (imaged) vortex dipole at $\zeta = 0$, so that $w(0) = -i$ (figure 2*b*). The points A, B, C, D of figure 2(*a*) map to the points A', B', C', D' of figure 2(*b*). Let

$$F(\zeta) = f(w(\zeta)) = f(z), \quad (2.12)$$

$$G(\zeta) = g(w(\zeta)) = g(z), \quad (2.13)$$

$$U(\zeta) = u_0(w(\zeta)) = u_0(z), \quad (2.14)$$

so that

$$f'(z) = \frac{F'(\zeta)}{w'(\zeta)}, \quad g'(z) = \frac{G'(\zeta)}{w'(\zeta)}. \quad (2.15)$$

Moreover, if $l (= \frac{1}{2}\pi - \theta)$ represents arclength from B' on the unit circle, then by the conformal mapping property $ds/dl = |w'(\zeta)|$, it follows that, for $z \in \Gamma$, i.e. $|\zeta| = 1$,

$$\frac{dz}{ds} = \frac{dw(\zeta)}{ds} = w'(\zeta) \frac{d\zeta dl}{dl ds} = -i\zeta \frac{w'(\zeta)}{|w'(\zeta)|}, \quad (2.16)$$

and equivalently

$$\left(\frac{dz}{ds}\right) = \frac{i \overline{w'(\zeta)}}{\zeta |w'(\zeta)|}. \quad (2.17)$$

Hence the boundary conditions (2.8) and (2.9) become

$$\frac{F'(\zeta)}{w'(\zeta)} + \overline{w(\zeta)} \frac{G'(\zeta)}{w'(\zeta)} - \overline{G(\zeta)} = U(\zeta) \frac{i \overline{w'(\zeta)}}{\zeta |w'(\zeta)|} \quad (2.18)$$

and

$$\frac{F'(\zeta)}{w'(\zeta)} + \overline{w(\zeta)} \frac{G'(\zeta)}{w'(\zeta)} + \overline{G(\zeta)} = \frac{\gamma \overline{w'(\zeta)}}{2\mu\zeta |w'(\zeta)|}. \quad (2.19)$$

Subtracting (2.18) from (2.19) and taking the complex conjugate gives

$$\frac{G(\zeta)}{\zeta w'(\zeta)} = \frac{1}{2|w'(\zeta)|} \left[\frac{\gamma}{2\mu} + iU(\zeta) \right] \quad \text{on } |\zeta| = 1. \quad (2.20)$$

Now $w'(\zeta)$ is analytic and non-zero in $|\zeta| < 1$, so that the left-hand side of (2.20) is analytic in $|\zeta| < 1$ except at $\zeta = 0$. To remove this singularity, we subtract $G(0)/\zeta w'(0)$ from each side of (2.20):

$$\frac{G(\zeta)}{\zeta w'(\zeta)} - \frac{G(0)}{\zeta w'(0)} = \frac{1}{2|w'(\zeta)|} \left[\frac{\gamma}{2\mu} + iU(\zeta) \right] - \frac{G(0)}{\zeta w'(0)} \quad \text{on } |\zeta| = 1. \quad (2.21)$$

Now, the left-hand side is the boundary value of a function analytic in $|\zeta| < 1$. If $w(\zeta)$ and $G(0)$ can be found, then the real part of the right-hand side of (2.21) will be known, so that then $G(\zeta)$ may be found.

The boundary conditions (2.3) and (2.11) transform in the ζ -plane to

$$F(\zeta) \sim \frac{\alpha i}{\zeta w'(0)} \quad \text{as } \zeta \rightarrow 0 \quad (2.22)$$

$$F(\zeta) = -\overline{w(\zeta)} G(\zeta) \quad \text{on } |\zeta| = 1. \quad (2.23)$$

These conditions together with the conditions (2.6) suggest the appropriate form for $w(\zeta)$. Note first that if the capillary number, which we now define as

$$\mathcal{C} = \mu\alpha/d^2\gamma, \quad (2.24)$$

is zero (i.e. $\gamma = \infty$), then the free surface is flat, so that the appropriate mapping would be the bilinear mapping

$$w_0(\zeta) = i \frac{\zeta - i}{\zeta + i}. \quad (2.25)$$

When $\mathcal{C} > 0$, the surface is distorted, but remains flat as $|x| \rightarrow \infty$ (i.e. as $\zeta \rightarrow -i$); we are therefore led to try a mapping function of the form

$$w(\zeta) = a(\zeta + i) + (a + 1)i \frac{\zeta - i}{\zeta + i}, \quad (2.26)$$

where a is a real constant to be determined. This mapping tends to bilinear form as $\zeta \rightarrow -i$, and satisfies the condition $w(0) = -i$ as required. (By guessing $w(\zeta)$ in the form

(2.26), the boundary condition (2.22) can also be satisfied, as will be seen later.) We shall find that, for suitable choice of a (dependent on the capillary number \mathcal{C}), we can satisfy all the conditions of the problem, so that (2.26) does indeed provide the required solution.

Note first that, from (2.26), $w(i) = 2ai$, so that the point $\zeta = i$ is the image of $z = 2ai$, the point B in figure 2(a). Since this must lie above the vortex dipole at $z = -i$, we must have $a > -\frac{1}{2}$. Secondly, the function

$$w'(\zeta) = a - \frac{2(a+1)}{(\zeta+i)^2} \quad (2.27)$$

must be non-zero in $|\zeta| < 1$. The zeros of $w'(\zeta)$ are at $\zeta = -i \pm (2(a+1)/a)^{\frac{1}{2}}$, and it is easily shown that both roots lie outside the unit circle if either $a < -1$ or $a > -\frac{1}{3}$. Together with the condition $a > -\frac{1}{2}$, we see therefore that the relevant range of a is

$$a > -\frac{1}{3}, \quad (2.28)$$

and we note that as $a \rightarrow -\frac{1}{3}$, a singularity appears on the boundary $|\zeta| = 1$ and hence on Γ also.

Substituting (2.26) in (2.23) (and using $\bar{\zeta} = 1/\zeta$) now gives

$$F(\zeta) = -\left\{ a\left(\frac{1}{\zeta} - i\right) + (a+1)i\frac{\zeta - i}{\zeta + i} \right\} G(\zeta). \quad (2.29)$$

Hence, as $\zeta \rightarrow 0$, $F(\zeta) \sim -aG(0)/\zeta$, so that comparing with (2.22) we find

$$G(0) = -\frac{\alpha i}{aw'(0)} = \frac{-\alpha i}{a(3a+2)}. \quad (2.30)$$

This provides a first relation between $G(0)$ and a . A second relation is needed to effect a complete solution. Note that $G(0)$ is pure imaginary.

Returning now to (2.21), the real part of the right-hand side is now known (apart from the real constant a). Hence by a well-known corollary of Cauchy's integral theorem (Muskhelishvili 1953) we have that, for $|\zeta| < 1$,

$$\frac{G(\zeta)}{\zeta w'(\zeta)} - \frac{G(0)}{\zeta w'(0)} = \frac{1}{2\pi i} \oint_{|\zeta_0|=1} \left[\frac{\gamma}{4\mu} \frac{1}{|w'(\zeta_0)|} - \operatorname{Re} \left\{ \frac{G(0)}{w'(0)} \frac{1}{\zeta_0} \right\} \right] \left(\frac{2}{\zeta_0 - \zeta} - \frac{1}{\zeta_0} \right) d\zeta_0 + ib, \quad (2.31)$$

where b is a real constant. The symmetry condition $\operatorname{Re} g(iy) = 0$ in fact implies that b must be zero. Evaluating the second term of the integral in (2.31) and rearranging, we thus obtain

$$\frac{G(\zeta)}{\zeta w'(\zeta)} = \frac{G(0)}{w'(0)} \left(\zeta + \frac{1}{\zeta} \right) + \frac{1}{2\pi i} \oint_{|\zeta_0|=1} \frac{\gamma}{4\mu |w'(\zeta_0)|} \frac{\zeta_0 + \zeta}{\zeta_0(\zeta_0 - \zeta)} d\zeta_0. \quad (2.32)$$

Consider now the behaviour of this expression as ζ tends to a point on the unit circle. With $\zeta_0 = e^{i\theta_0}$ and $\zeta = e^{i\theta}$, we have from (2.32)

$$\frac{G(\zeta)}{\zeta w'(\zeta)} = 2 \cos \theta \frac{G(0)}{w'(0)} + \frac{\gamma}{4\mu} \frac{1}{|w'(\zeta)|} + \frac{\gamma i}{8\pi\mu} \int_0^{2\pi} \frac{1}{|w'(e^{i\theta_0})|} \frac{\cos \theta_0 + \cos \theta}{\sin \theta - \sin \theta_0} d\theta_0. \quad (2.33)$$

Recalling that $G(0)$ is pure imaginary, we see that the real part of this expression is $\gamma/4\mu|w'(\zeta)|$ as required by (2.20). Comparing the imaginary parts of (2.20) and (2.33) we obtain an expression for the tangential free-surface velocity:

$$\begin{aligned} u_0(z) &= U(\zeta) = U(e^{i\theta}) \\ &= -\cos \theta |w'(e^{i\theta})| \left[\frac{4G(0)}{w'(0)} i + \frac{\gamma}{4\pi\mu} \int_0^{2\pi} \frac{1}{|w'(e^{i\theta_0})|} \frac{d\theta_0}{\sin \theta_0 - \sin \theta} \right]. \end{aligned} \quad (2.34)$$

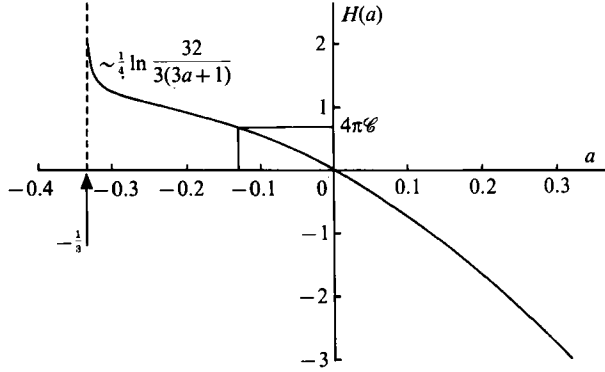


FIGURE 3. Graph of the function $H(a)$ defined by (2.39). For each value of the capillary number \mathcal{C} (positive or negative) the real parameter a is uniquely determined by $H(a) = 4\pi\mathcal{C}$ (equation (2.38)).

Now, from (2.27), we may obtain

$$|w'(e^{i\theta})|^2 = a^2 + 2a(a+1) \frac{\sin \theta}{1 + \sin \theta} + \left(\frac{a+1}{1 + \sin \theta} \right)^2. \quad (2.35)$$

Hence $u_0(z)$ is given explicitly in terms of the parameter a , which is still unknown.

This parameter may now however be determined from the condition that $u_0(z) \rightarrow 0$ as $z \rightarrow \pm\infty$ (i.e. as $\theta \rightarrow -\frac{1}{2}\pi$ in (2.34)). Near $\theta = -\frac{1}{2}\pi$, we have

$$\cos \theta |w'(e^{i\theta})| \sim |a+1| \frac{\cos \theta}{|1 + \sin \theta|} \sim 2 \frac{|a+1|}{|\frac{1}{2}\pi + \theta|}. \quad (2.36)$$

Hence the term in square brackets in (2.34) must certainly vanish as $\theta \rightarrow -\frac{1}{2}\pi$, i.e.

$$G(0) = \frac{i\gamma w'(0)}{16\pi\mu} \int_0^{2\pi} \frac{d\theta_0}{|w'(e^{i\theta_0})| (\sin \theta_0 + 1)}. \quad (2.37)$$

(Note that, since (2.36) has a simple pole and the term in square brackets in (2.34) has a double zero, $u_0(z)$ does indeed tend to zero at infinity.)

Substituting (2.26), (2.30) and (2.35) into (2.37), we obtain an equation of the form

$$H(a) = \frac{4\pi\mu\alpha}{\gamma} = 4\pi\mathcal{C} \quad (2.38)$$

from which a may be determined. The function $H(a)$ is given (see Appendix A) by

$$H(a) = \begin{cases} \frac{-a(3a+2)^2}{(1+a+(-2a(a+1))^{\frac{1}{2}})^{\frac{1}{2}}} K(m) & \text{for } -\frac{1}{3} < a \leq 0, \\ \frac{-a(3a+2)^2}{((a+1)(3a+1))^{\frac{1}{2}}} K(m') & \text{for } a \geq 0, \end{cases} \quad (2.39)$$

where

$$m = \frac{2}{(-2a/(a+1))^{\frac{1}{2}} + ((a+1)/(-2a))^{\frac{1}{2}}}, \quad m' = \left(\frac{2a}{3a+1} \right)^{\frac{1}{2}}, \quad (2.40)$$

and K is the complete elliptic integral of the first kind:

$$K(m) = \int_0^{\frac{1}{2}\pi} \frac{d\theta}{(1-m^2 \sin^2 \theta)^{\frac{1}{2}}} = \int_0^1 \frac{dx}{[(1-x^2)(1-m^2 x^2)]^{\frac{1}{2}}}. \quad (2.41)$$

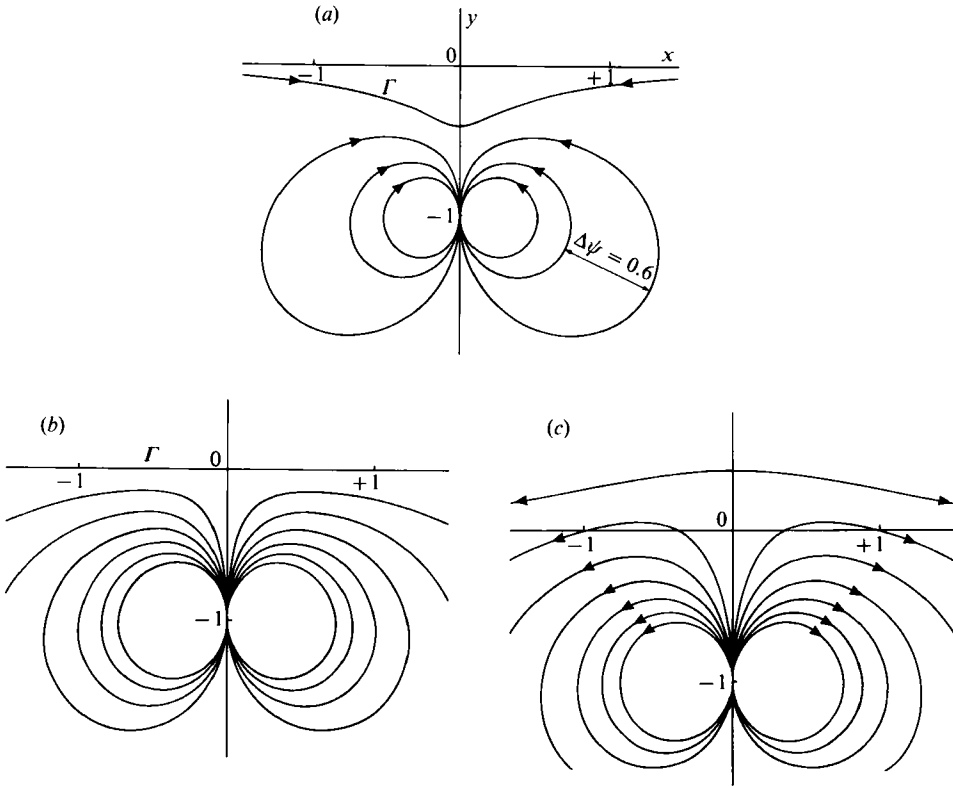


FIGURE 4. Streamlines and corresponding free-surface shape for various values of a . All streamlines pass through the singularity at $(0, -1)$, and the streamlines near this point are circles touching the y -axis. (a) $a = -0.2$, $\mathcal{C} = 0.072$; (b) $a = 0$, $\mathcal{C} = 0$ (potential flow with undisturbed free surface); (c) $a = 0.2$, $\mathcal{C} = -0.13$; in this case ($\alpha < 0$) the flow is diverging on Γ and the free surface is pushed upwards.

The function $H(a)$ as given by (2.39) has been computed and is shown in figure 3. The asymptotic behaviour of this function is easily calculated:

$$H(a) = -2\pi a(1 + \frac{3}{2}a) + O(a^3) \quad \text{for } a \ll 1, \quad (2.42)$$

$$H(a) \sim -Ca^2, \quad C = 3^{\frac{3}{2}}K((\frac{2}{3})^{\frac{1}{2}}) \approx 10.54 \quad \text{as } a \rightarrow \infty, \quad (2.43)$$

$$H(a) \sim \frac{1}{4} \ln \frac{32}{3(3a+1)} \quad \text{as } a \rightarrow -\frac{1}{3}. \quad (2.44)$$

For given capillary number \mathcal{C} , the parameter a is uniquely determined by (2.38). Note that for $\mathcal{C} \geq 0$, a lies in the range $-\frac{1}{3} \leq a \leq 0$, while for $\mathcal{C} < 0$ (corresponding to $\alpha < 0$), $a > 0$.

With a known, we can now complete the solution of the problem. First, from (2.32) and (2.37), we derive

$$G(\zeta) = -\frac{\alpha}{8H(a)} w'(\zeta) \left(\zeta + \frac{1}{\zeta} \right) (\zeta + i)^2 I \left(\frac{\zeta - \zeta^{-1}}{2i}; a \right), \quad (2.45)$$

where

$$\begin{aligned} I(\zeta; a) &= \int_0^{2\pi} \frac{d\theta_0}{|w'(e^{i\theta_0})| (\sin \theta_0 + 1) (\sin \theta_0 - \zeta)} \\ &= \int_{-1}^1 \frac{2 dt}{(t - \zeta) (1 - t^2)^{\frac{1}{2}} [a(3a + 2)t^2 + 2a(2a + 1)t + a^2 + (a + 1)^2]^{\frac{1}{2}}}. \end{aligned} \quad (2.46)$$

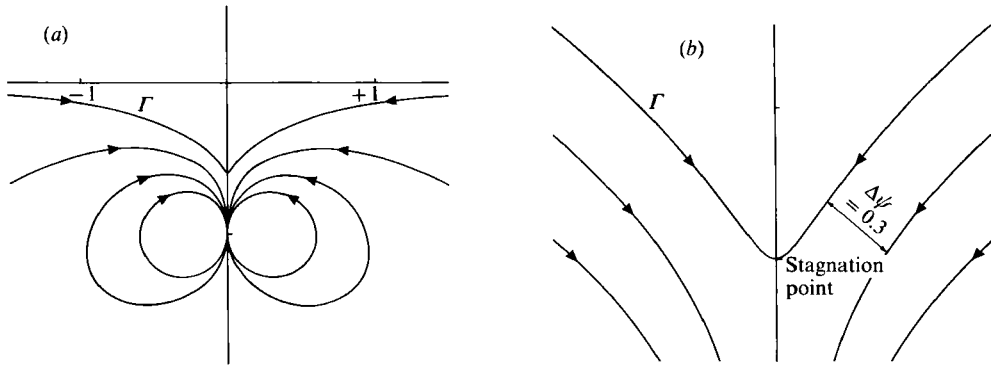


FIGURE 5. (a) As for figure 4, but with $a = -0.3$, $\mathcal{C} = 0.1$; (b) same figure expanded around the stagnation point on Γ .

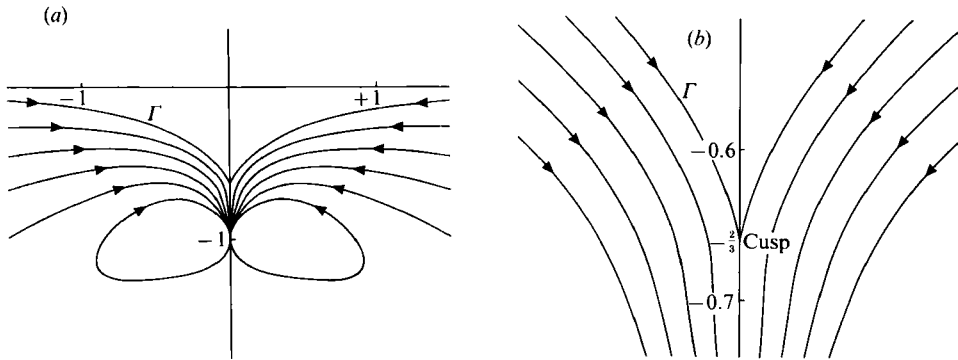


FIGURE 6. (a) As for figure 4, but with $a = -\frac{1}{3}$, $\mathcal{C} = \infty$; (b) same figure expanded around the cusp on Γ .

This integral can be expressed in terms of complete elliptic integrals of the first and third kinds (see Appendix A). Now from (2.2), (2.12), (2.13) and (2.29), the stream function ψ is given in terms of $G(\zeta)$ by

$$\psi = \text{Im} \left[G(\zeta) \left\{ a(\bar{\zeta} - \zeta^{-1}) - 2(a+1) i \frac{\zeta \bar{\zeta} - 1}{|\zeta + i|^2} \right\} \right] \quad (2.47)$$

from which the streamlines $\psi = \text{const.}$ may be plotted. Figures 4–6 show the streamlines for a range of values of a (with corresponding values of \mathcal{C} from figure 3). Note in particular the tendency to form a cusp as $a \rightarrow -\frac{1}{3}$ ($\mathcal{C} \rightarrow \infty$).

3. The free surface

The free surface Γ is given by $z = w(\zeta)$ with $\zeta = e^{i\theta}$, or, from (2.26),

$$z = a(e^{i\theta} + i) + (a+1) i \frac{e^{i\theta} - i}{e^{i\theta} + i}. \quad (3.1)$$

The real and imaginary parts give the equation of Γ in parametric form:

$$x = a \cos \theta + (a+1) \frac{\cos \theta}{1 + \sin \theta}, \quad (3.2a)$$

$$y = a(1 + \sin \theta). \quad (3.2b)$$

Elimination of θ gives the equation of Γ as the cubic curve

$$x^2y = (2a - y)(y + a + 1)^2. \quad (3.3)$$

This curve is sketched in figure 7 for a range of values of a ; only the range $a \geq -\frac{1}{3}$ is relevant to the problem studied here. When $a = -\frac{1}{3}$, the curve has a cusp with vertical tangent at $x = 0$, $y = -\frac{2}{3}$.

For $a > -\frac{1}{3}$, the curve is locally parabolic near the point $(0, 2a)$:

$$x^2 \approx \frac{(3a + 1)^2}{-2a}(y - 2a). \quad (3.4)$$

The radius of curvature at $(0, 2a)$ is

$$R = (3a + 1)^2 / (-4a). \quad (3.5)$$

As $a \rightarrow -\frac{1}{3}$, the asymptotic form (2.44) together with (2.38) now gives $(3a + 1) \sim \frac{32}{3} \exp\{-16\pi\mathcal{C}\}$; hence, restoring the dimensional length d , R is given asymptotically by

$$R/d \sim \frac{256}{3} \exp\{-32\pi\mathcal{C}\}, \quad (3.6)$$

as stated in the Introduction. This asymptotic behaviour is reasonably accurate for $\mathcal{C} \gtrsim 0.1$ ($H(a) \gtrsim 1.2$ in figure 3), and indicates extremely small values of R/d when \mathcal{C} is of order unity. Even for $\mathcal{C} = 0.1$, we have $R/d \approx 3.67 \times 10^{-3}$, while for $\mathcal{C} = 0.25$, $R/d \approx 10^{-9}$, and for $\mathcal{C} = 1$, $R/d \approx 1.87 \times 10^{-42}$! Of course the continuum approximation fails on such small lengthscales; from a continuum point of view, it seems fair to state that when d is of order 1 m or less, a cusp does indeed form when $\mathcal{C} \gtrsim 0.25$ (giving $R/d \lesssim 10^{-9}$).

Putting $a = -\frac{1}{3} + \epsilon$, we find from (3.3) that for $\epsilon \ll 1$ and $y + \frac{2}{3} \gg \epsilon$, the free-surface shape is

$$x^2y \approx -(y + \frac{2}{3})^3. \quad (3.7)$$

If we further restrict y to the range for which $\epsilon \ll y + \frac{2}{3} \ll 1$ (so that $y \approx -\frac{2}{3}$), then (3.7) gives

$$x^2 \approx \frac{3}{2}Y^3, \quad Y = y + \frac{2}{3}, \quad (3.8)$$

in agreement with the self similar form $x \sim \bar{c}Y^{\frac{3}{2}}$ obtained by JNRR, but with the added bonus that the coefficient \bar{c} , which is undetermined in JNRR's local analysis, is here determined as $\bar{c} = (\frac{3}{2})^{\frac{1}{2}} \approx 1.225$. This value of \bar{c} is particular to the idealized vortex dipole problem; in more general experimental configurations, \bar{c} may be expected to depend on the dimensionless parameters defining the geometry (e.g. r_c/d in the configuration of figure 1a). JNRR used a coordinate system in which the cusp opened along the negative x -axis, and their result, equivalent to (3.8) was $y \sim \bar{c}x^{\frac{2}{3}}$. Their experiments with STP, silicone oil and castor oil showed qualitative agreement with this theory, but the value of \bar{c} was ill-determined. The capillary number used by JNRR is (using (3.12)) approximately 16 times the \mathcal{C} that we use in the present paper; hence the value $\mathcal{C} = 0.25$ corresponds to $[\mathcal{C}]_{\text{JNRR}} \approx 4$, in rough agreement with their critical value for cusp formation.

In spite of the dependence of \bar{c} on the geometry, the curves (3.7) and (3.8) when superposed on the photograph obtained in our experiment (figure 8) at a capillary number $(\mathcal{C})_{\text{exp}} = \mu\Omega r_c/\gamma \approx 60$ exhibit a remarkable convergence to the observed form of the cusp. Agreement is not to be expected far from the cusp where the precise geometry of the experiment must certainly have some influence. The imperfection of the fit between theory and experiment at the very tip of the cusp may be due to imperfect scaling of the photograph.

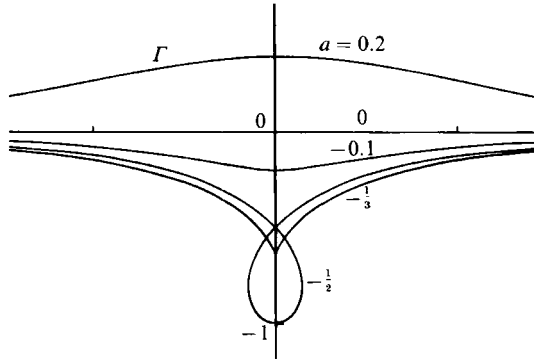


FIGURE 7. The curve (3.3) for $a = -\frac{1}{2}, -\frac{1}{3}, -0.1, 0, +0.2$. Only the curves corresponding to $a \geq -\frac{1}{3}$ are physically relevant here. The curve is cusped for $a = -\frac{1}{3}$. For $a \geq -\frac{1}{3}$, the curve provides the free-surface shape at the capillary number \mathcal{C} given by figure 3.

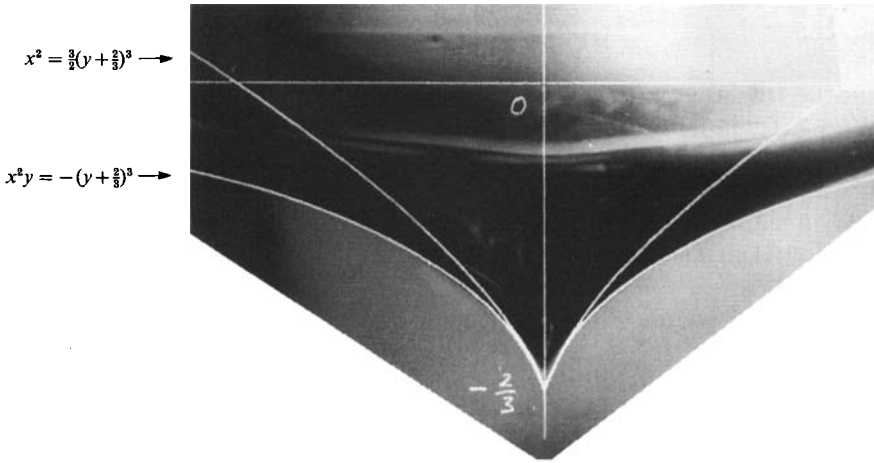


FIGURE 8. The asymptotic curves (3.7) and (3.8) superposed on the observed cusp in an experiment with $\mathcal{C}_{\text{exp}} = 52.4$. The photograph is enlarged to give the best fit with the curve $x^2 y = -(y + \frac{2}{3})^3$.

The curve (3.3) has a universal form when $a = -\frac{1}{3} + \epsilon$, $0 < \epsilon \ll 1$. This is obtained by the substitutions

$$x = \epsilon^{\frac{3}{2}} \xi, \quad Y = y - 2a = \epsilon \eta. \quad (3.9)$$

Retaining only leading-order contributions (of order ϵ^3), this yields the curve

$$\xi^2 = \frac{3}{2} \eta (\eta + 3)^2, \quad (3.10)$$

which exhibits the parabolic behaviour $\xi^2 \sim \frac{3}{2} \eta$ for $\eta \ll 1$, and the cuspidal behaviour $\xi^2 \sim \frac{3}{2} \eta^3$ for $\eta \gg 1$ (figure 9). The curve (3.10) has inflexion points at $\eta = 1$, $\xi = \pm 2\sqrt{6}$ marking the transition between these regimes.

Consider now the tangential velocity $u_0(z)$ on Γ , which is given from (2.34) and (2.37) by

$$\frac{1}{\alpha} u_0(z) = \frac{1}{\alpha} U(e^{i\theta}) = -\frac{1}{4\pi\mathcal{C}} (1 + \sin \theta) \cos \theta |w'(e^{i\theta})| I(\sin \theta; a) \quad (3.11)$$

where I is still as defined by (2.46) (where the principal value must now be used). With θ related to x by (3.2a), (3.11) determines u_0/α implicitly as a function of x . This function is shown in figure 10 for various values of a in the range

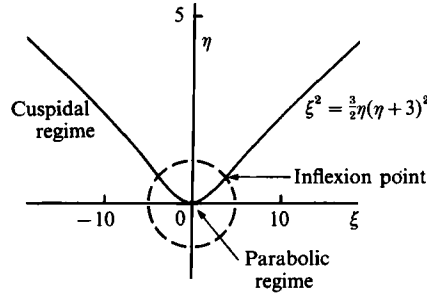


FIGURE 9. The universal curve $\xi^2 = \frac{3}{2}\eta(\eta + 3)^2$ representing transition from parabolic to cuspidal regimes.

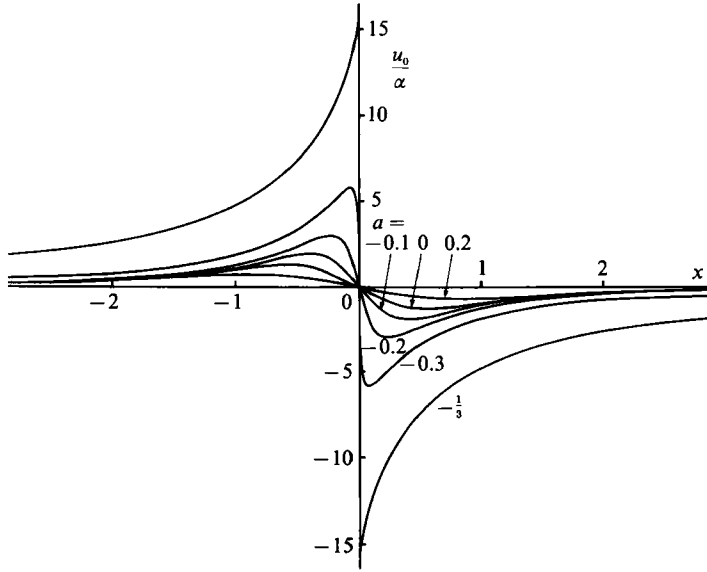


FIGURE 10. The tangential velocity $u_0(x)$ on Γ normalized with respect to the strength α of the vortex dipole, for $a = -\frac{1}{3}, -0.3, -0.2, -0.1, 0, 0.2$. Note the singular structure as $a \rightarrow -\frac{1}{3}$, and the limiting value $u_0(0)/\alpha = \pm 16$.

$-\frac{1}{3} \leq a \leq 0.2$ ($\infty \geq \mathcal{C} \geq -0.13$). The curve corresponding to $a = 0$ coincides with that obtained by a linearized analysis (Appendix B, equation (B 16)). The free-surface velocity is directed towards or away from the stagnation point on the free surface according as $a < 0$ or $a > 0$. A singular structure is evident as $\epsilon = a + \frac{1}{3} \rightarrow 0$, with rapid deceleration in the region $|x| = O(\epsilon^{\frac{2}{3}})$ where the cuspidal shape of the free surface gives way to the parabolic shape. Note the limiting behaviour

$$\lim_{|x| \rightarrow 0} \lim_{\epsilon \rightarrow 0} (u_0/\alpha) = \pm 16, \tag{3.12}$$

indicating that the (dimensional) fluid velocity through the cusp into the fluid interior has magnitude $16\alpha/d^2$. As noted above, for any capillary number greater than about 0.25, the parameter ϵ is extremely small, and this limiting description must certainly be appropriate.

We may note that, when $\mathcal{C} \gtrsim 0.25$, the 'parabolic region' is on a submicron scale, so that the question of whether fluid particles on the free surface do or do not move

into the interior of the fluid has a rather philosophical character. In situations such as this where the continuum approximation breaks down, the concept of a fluid particle is ill-defined, and the true behaviour in the neighbourhood of the cusp must surely require consideration of intermolecular forces and related non-continuum effects. The same comment applies to the behaviour of the air trapped in the cusp region. These considerations are unlikely, however, to affect the 'outer' cusp dynamics, and the shape of the cusp as given by (3.8).

4. Asymptotic form of stream function as $a \rightarrow -\frac{1}{3}$

We have already seen in (2.44) that the function $H(a)$ has a logarithmic singularity as $a \rightarrow -\frac{1}{3}$ (i.e. $\mathcal{C} \rightarrow \infty$). The same singularity appears in the function $I((\zeta - \zeta^{-1})/2i; a)$ appearing in the solution for $G(\zeta)$ (equation (2.45)):

$$I\left(\frac{\zeta - \zeta^{-1}}{2i}; a\right) \sim -\frac{6i\zeta}{(\zeta - i)^2} \ln \frac{32}{3(3a + 1)} \quad \text{as } a \rightarrow -\frac{1}{3} \quad (4.1)$$

(see Appendix A). Hence from (2.45),

$$G(\zeta) \sim -i\alpha(\zeta + 3i)(\zeta + i), \quad (4.2)$$

and so from (2.47),

$$\psi \sim \text{Im} \left[\frac{i}{3} \alpha(\zeta + 3i)(\zeta + i)(\zeta\bar{\zeta} - 1) \left\{ \frac{1}{\zeta} + \frac{4i}{|\zeta + i|^2} \right\} \right], \quad (4.3)$$

with ζ related to z , when $a = -\frac{1}{3}$, by

$$z = -\frac{1}{3}(\zeta + i) + \frac{2i}{3} \frac{\zeta - i}{\zeta + i}. \quad (4.4)$$

Near the cusp point $\zeta = i$ ($z = -\frac{2}{3}i$), (4.4) becomes

$$z + \frac{2}{3}i \approx \frac{i}{6}(\zeta - i)^2 + \dots \quad (4.5)$$

and, with $z + \frac{2}{3}i = ir e^{i\theta}$ (so that r is distance from the cusp and θ is measured from the direction of the cusp tangent), (4.3) gives the asymptotic form of ψ near the cusp as

$$\psi \sim 16\alpha x - 8\sqrt{6}\alpha r^{\frac{3}{2}} \sin^3\left(\frac{1}{2}\theta\right) \quad (-\pi \leq \theta \leq \pi), \quad (4.6)$$

agreeing with the local similarity solution proposed by JNRR (at least when $\mathcal{C} = \infty$). This stream function represents the uniform stream -16α into the fluid, with a superposed perturbation velocity of order $r^{\frac{1}{2}}$ near $r = 0$. Note however that the associated rate of strain is $O(r^{-\frac{1}{2}})$. This is resolved on the scale $r = O(\epsilon) = O(e^{-16\pi\mathcal{C}})$. Hence a maximum strain rate of order $e^{8\pi\mathcal{C}}$ is implied. The corresponding stress in the fluid is extremely large for quite modest values of \mathcal{C} . However, the $O(r^{-1})$ singularity in the rate of viscous dissipation is integrable.

5. Influence of gravity

It is obvious that, in an experiment like that of figure 1, gravity exerts a stabilizing influence on the free surface, tending to keep it horizontal against the influence of viscous stresses. The effect of gravity was neglected in the model problem of §2. We may however estimate its effect by a local stability analysis similar to that used by Lister (1989) in a rather similar axisymmetric situation.

We consider the stability of the free surface $y = 0$ under the action of the converging uniform strain

$$U = (-sx, sy). \quad (5.1)$$

Consider a disturbance of the free surface of the form

$$y = \eta(x, t) = \hat{\eta}(t) e^{ik(t)x}. \quad (5.2)$$

It is obvious that

$$k(t) = k_0 e^{st}, \quad (5.3)$$

due to the compression of the wave-form (figure 11 *a*). If gravity and surface tension were absent, then the disturbance amplitude $\hat{\eta}(t)$ would also increase as e^{st} , a purely kinematic effect. Both gravity and surface tension have a countervailing influence.

The stream function $\psi(x, y, t)$, satisfying $\nabla^4 \psi = 0$ and $\psi \rightarrow 0$ as $y \rightarrow -\infty$, may readily be shown to have the form

$$\psi = (A + By) e^{ky} e^{ikx}, \quad (5.4)$$

and the (linearized) kinematic boundary condition $DF/Dt = 0$ on $y = \eta(x, t)$ where $F \equiv y - \eta(x, t)$ gives

$$\frac{d\hat{\eta}}{dt} = s\hat{\eta} - ikA. \quad (5.5)$$

The tangential stress is zero on $y = \eta$; hence

$$B = -2is\hat{\eta}. \quad (5.6)$$

The linearized normal stress condition $\sigma_{nn} = \gamma \partial^2 \eta / \partial x^2$ on $y = \eta$ yields

$$2ik^2 \mu A = (\gamma k^2 + \rho g) \hat{\eta}. \quad (5.7)$$

Hence, from (5.5) and (5.7),

$$\frac{d\hat{\eta}}{dt} = \frac{(\rho g \gamma)^{\frac{1}{2}}}{\mu} \Sigma(K) \hat{\eta}, \quad (5.8)$$

where $\Sigma = S - \frac{1}{2}(K + K^{-1})$, $S = \frac{s\mu}{(\rho g \gamma)^{\frac{1}{2}}}$, $K = \left(\frac{\gamma}{\rho g}\right)^{\frac{1}{2}} k$. (5.9)

The form of the curve $\Sigma = \Sigma(K)$ is shown in figure 11 (*b*) for various values of S . Note that $\Sigma_{\max} = S - 1$, so that Σ is positive for a range of wavenumbers if

$$S > 1. \quad (5.10)$$

As a disturbance of initially large wavelength (small k) is compressed, it is then exponentially amplified as its wavenumber $k(t)$ passes through this unstable range. We may regard (5.10) as a *necessary condition* for the development of a finite-amplitude disturbance of the interface in a neighbourhood of $x = 0$.

If the condition (5.10) is satisfied, and if a depression of the free surface forms at $x = 0$, then the local strain rate tends to increase. In fact, as discussed in §4, a maximum strain rate of order $\alpha d^{-3} e^{8\pi\epsilon}$ may be expected in the parabolic region. This suggests that when the disturbance grows into the nonlinear regime, the local strain rate s may in fact increase in such a way as to keep in step with the increasing effect of surface tension near the stagnation point. Certainly, gravity becomes insignificant in this neighbourhood, and the results of the previous sections may be expected to be asymptotically valid near $x = 0$ even when gravity is present.

Note that, as shown in figure 13 and described in the following section, it is also possible for a crest to appear at $x = 0$ when the strain rate s is small. The linearized analysis of Appendix B indicates that this occurs when the horizontal separation of

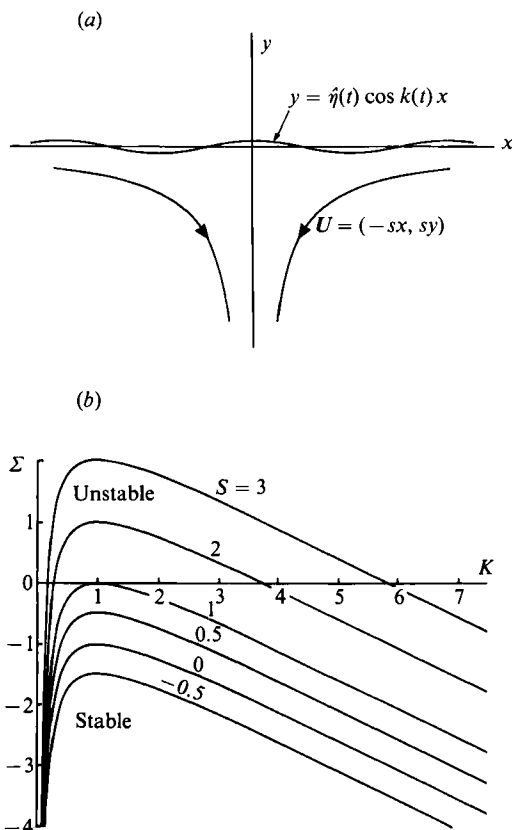


FIGURE 11. (a) Compression of free-surface wave form under the action of uniform strain; (b) the dispersion relation (5.9) showing an unstable range of wavenumbers when the condition (5.10) is satisfied.

the vortices representing the rotating cylinders is greater than $2d$. The shape of the crest is (presumably) influenced by both gravity and surface tension.

6. Experimental details

The experiment depicted in figure 1 was carried out in a Perspex box of horizontal dimensions 250×250 mm. The radius of each cylinder is $r_c = 23$ mm and the separation of centres is $2c = 100$ mm. The depth of fluid d is of course variable; we used $d = 40$ mm for the experiment described here. The speed of rotation of the two cylinders can be independently varied, but we focus here on the symmetric situation with angular velocities $\pm\Omega$, and Ω in the range zero to approximately 7 s^{-1} . The Froude number $Fr = \Omega(r_c/g)^{1/2}$ was then in the range $[0, 0.34]$.

The fluid used was a reasonably Newtonian polybutene of density $\rho = 883 \text{ kg m}^{-3}$, viscosity $\mu = 12.9 \text{ kg m}^{-1} \text{ s}^{-1}$ and surface tension $\gamma = 0.034 \text{ N m}^{-1}$. The range of Reynolds numbers $Re = \rho\Omega r_c^2/\mu$, was $[0, 0.25]$, so that the low-Reynolds-number approximation $Re \ll 1$ is applicable. The range of capillary number $\mathcal{C}_{\text{exp}} = \mu\Omega r_c/\gamma$ was $[0, 61.1]$. The flow is accurately two-dimensional except in layers on the front and rear walls of the box where the no-slip condition is satisfied. The free surface was illuminated by a weak diffuse source of light from behind the box and this enabled photographs of the free surface shape with the camera positioned as in figure 12.

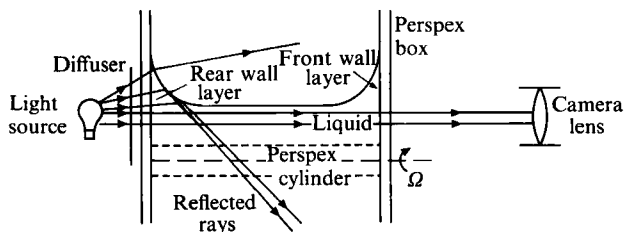


FIGURE 12. Configuration of light source and camera in the experiment; note that the total internal reflection of light from the free surface in the rear-wall layer means that no light reaches the camera lens from the region of air immediately above the free surface.

Total internal reflection of light from the free surface in the rear boundary layer means that no light gets to the camera from the air just above the free surface, and this region therefore appears black in the photographs. The ratio $\mathcal{C}_{\text{exp}}/Fr = \mu(r_c g)^{1/2}/\gamma$ had the value 180.

The sequence of photographs (*a-h*) in figure 13 shows the effect of increasing the angular velocity slowly from zero. For small values of Ω , there is a crest at $x = 0$, and as Ω increases this crest is progressively more concentrated near $x = 0$. As Ω approaches a critical value Ω_c , the crest disappears and for $\Omega > \Omega_c$, a downward-pointing cusp appears on the free surface. The Froude number at which this transition took place was $Fr_c = 0.136$, and the capillary number was $\mathcal{C} \approx 24$. With further increase of Ω , the cusp becomes more pronounced, but there is no further qualitative change in the flow structure for the range of Ω covered by this experiment. Further experiments using a range of different fluids, and varying the cylinder radius r_c , are needed to determine the locus in the (Fr, \mathcal{C}) -plane where the transition from crest to cusp occurs.

As indicated previously (figure 8), the form of the cusp is well represented by the equation $x^2 = c^2 Y^3$ with $c = (\frac{3}{2})^{1/2}$ (although since this value of c was determined for the idealized dipole configuration, the agreement is to some extent fortuitous).

The similarity solution for cusp flow given by JNRR gave a cusp of the form $x \sim cY^\lambda$ where λ is a function of \mathcal{C} tending to $\frac{3}{2}$ as $\mathcal{C} \rightarrow \infty$. Our exact solution of the vortex dipole problem gives $\lambda = \frac{3}{2}$ even for finite \mathcal{C} (see the universal behaviour of figure 9); this means that the flow in the immediate neighbourhood of the cusp (i.e. the parabolic region) has an important effect on the cuspidal region where the free-surface behaviour $x \sim cY^{3/2}$ is valid. There are some similarities here with the problem of viscous fingering (Saffman 1986), for which the gross properties of the fingers are sensitively dependent on conditions very near the tip.

This work was motivated by observations of a flow exhibiting what looked like a cusp during a visit of one of us (H.K.M) to the Ecole Normale Supérieure in Lyon at the invitation of Stefan Fauve in June 1990. The work described in §§5 and 6 of this paper was presented at the British Theoretical Mechanics Colloquium in Oxford in April 1991, and we gratefully acknowledge the helpful comments of Philip Drazin, Alex Craik and others following this presentation; also the equally helpful comments of John Lister and other colleagues at DAMTP who have taken an interest in the experiment. We thank David Cheesley for helping in the design of the experiment and for constructing the apparatus; and Jason Newling for help with the photography. J.-T.J. has been financed by a Fellowship of the Korea Science and Engineering Foundation 1990.

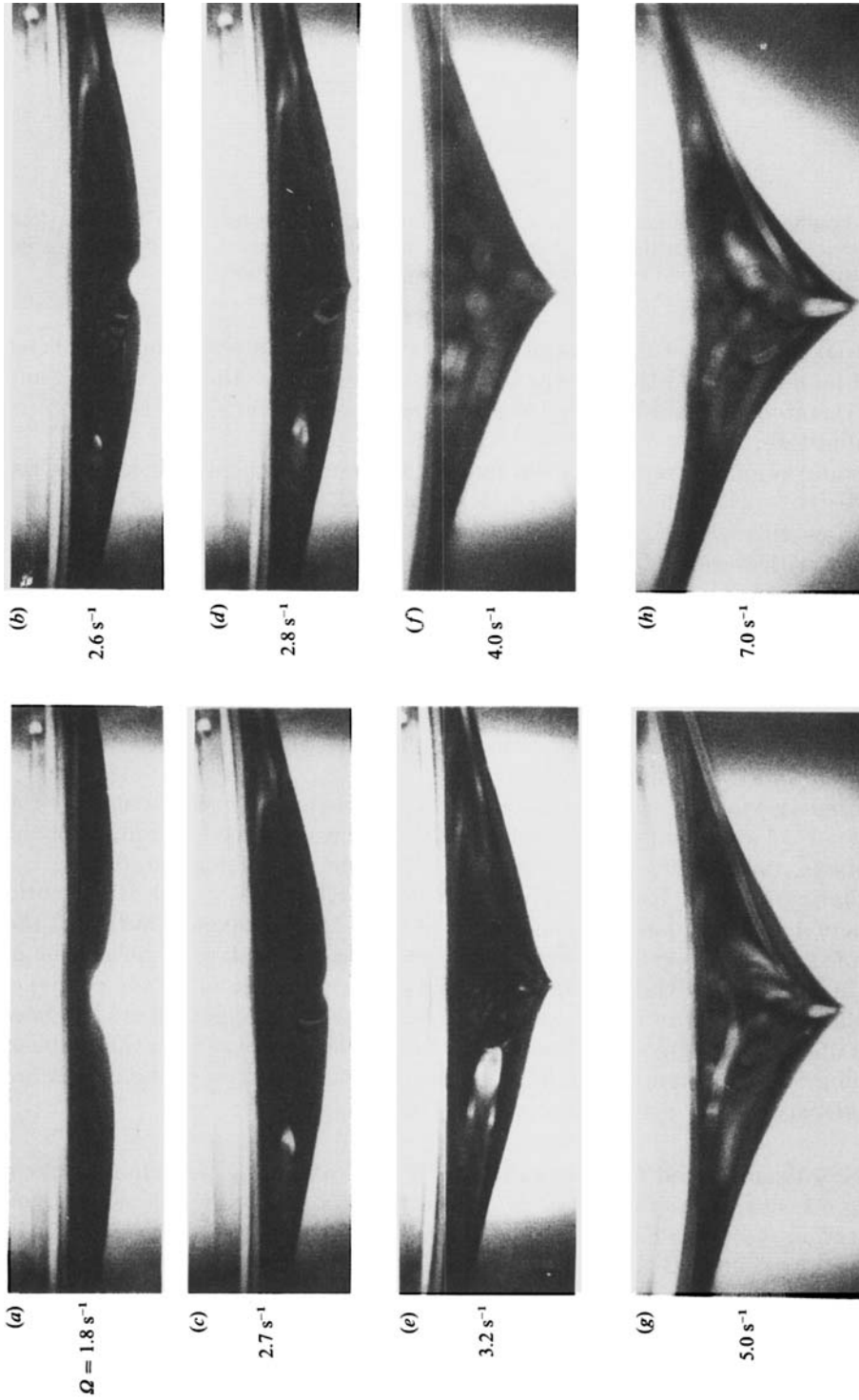


FIGURE 13. Sequence of photographs showing the transition from crest to cusp as Ω is increased through a critical value $\Omega_c \approx 2.75 \text{ s}^{-1}$. The capillary number $\mathcal{G}_{\text{exp}} = \mu\Omega r_c/\gamma$ has the following values: (a) 15.7; (b) 22.7; (c) 23.6; (d) 24.4; (e) 27.9; (f) 34.9; (g) 43.6; (h) 61.1. The horizontal extent of the free surface shown in each of these photographs is approximately 5 cm.

Appendix A. Calculation of some integrals required in §2

Substituting $w'(0) = 3a + 2$ from (2.27), $G(0)$ from (2.30), and (2.35) into (2.37), we obtain $H(a) = 4\pi\mu\alpha/\gamma$ where

$$H(a) = -\frac{1}{4}a(3a+2)^2 \int_0^{2\pi} \frac{d\theta_0}{[a(3a+2)\sin^2\theta_0 + 2a(2a+1)\sin\theta_0 + a^2 + (a+1)^2]^{\frac{1}{2}}}. \quad (\text{A } 1)$$

Evaluating the integral (see, for example, Gradshteyn & Ryzhik 1980), (A 1) can be reduced to (2.39). Now, consider (2.46), where the integral can be expressed in terms of complete elliptic integrals as follows

$$I(\zeta; a) = \int_{-1}^1 \frac{2 dt}{(t-\zeta)(1-t^2)^{\frac{1}{2}}[a(3a+2)t^2 + 2a(2a+1)t + a^2 + (a+1)^2]^{\frac{1}{2}}} \\ = \begin{cases} \frac{4}{(t_1-\zeta)\{a+1+(-2a(a+1))^{\frac{1}{2}}\}} \left[K(m) - \frac{t_1+1}{\zeta+1} \Pi(n, m) \right] & \text{for } -\frac{1}{3} < a \leq 0, \\ \frac{-4}{(a\zeta+2a+1)\{(a+1)(3a+1)\}^{\frac{1}{2}}} \left[aK(m') + \frac{a+\zeta(2a+1)}{\zeta^2-1} \Pi(q, m') \right] & \text{for } a \geq 0, \end{cases} \quad (\text{A } 2)$$

where

$$t_1 = \frac{-a(2a+1) + (a+1)(-2a(a+1))^{\frac{1}{2}}}{a(3a+2)} \\ n = \frac{2(\zeta-t_1)}{(\zeta+1)(1-t_1)}, \quad q = \frac{(a\zeta+2a+1)^2}{(1-\zeta^2)(a+1)(3a+1)},$$

and m, m' are defined in (2.40). In (A 2), $K(m)$ and $\Pi(n, m)$ are complete elliptic integrals of the first and third kinds (Gradshteyn & Ryzhik 1980; Byrd & Friedman 1971):

$$K(m) = \int_0^{\frac{1}{2}\pi} \frac{d\theta}{(1-m^2\sin^2\theta)^{\frac{1}{2}}} = \int_0^1 \frac{dx}{[(1-x^2)(1-m^2x^2)]^{\frac{1}{2}}}, \\ \Pi(n, m) = \int_0^{\frac{1}{2}\pi} \frac{d\theta}{(1-n\sin^2\theta)(1-m^2\sin^2\theta)^{\frac{1}{2}}} = \int_0^1 \frac{dx}{(1-nx^2)[(1-x^2)(1-m^2x^2)]^{\frac{1}{2}}}.$$

Appendix B. Linearized analysis for a small perturbation of the free surface

Consider the flow due to vortices of strengths $\pm\kappa$ placed at $(\mp c, -1)$ respectively, in otherwise quiescent fluid. Suppose that the free surface is $y = \eta(x)$, where $\eta(\pm\infty) = 0$ and η and η' are both assumed small. We include here the effects of both gravity and surface tension, represented by the non-dimensional numbers

$$G = \rho g/2\mu\kappa, \quad \mathcal{C} = 2\mu\kappa/\gamma. \quad (\text{B } 1)$$

The linearized form of the boundary conditions at the free surface is

$$\psi = 0, \quad \sigma_{xy} = 0 \quad \text{on } y = 0, \quad (\text{B } 2)$$

and
$$\sigma_{yy} = \gamma \eta''(x) \quad \text{on } y = \eta(x), \quad (\text{B } 3)$$

where
$$(\sigma_{yy})_{y=\eta} \approx -(p)_{y=\eta} + 2\mu(\partial v/\partial y)_{y=0} = \rho g \eta - 2\mu(\partial^2 \psi/\partial x \partial y)_{y=0}. \quad (\text{B } 4)$$

With image vortices $\pm \kappa$ at $(\pm c, 1)$ respectively, the stream function for the (potential) flow satisfying (B 2) is

$$\psi(x, y) = \frac{1}{2} \kappa \ln \frac{\{(x-c)^2 + (y-1)^2\} \{(x+c)^2 + (y+1)^2\}}{\{(x+c)^2 + (y-1)^2\} \{(x-c)^2 + (y+1)^2\}} \quad (\text{B } 5)$$

and the conditions (B 3), (B 4) may then be combined to give the equation for $\eta(x)$:

$$\mathcal{C}^{-1} \eta'' - G \eta = -\kappa^{-1} du_0/dx, \quad (\text{B } 6)$$

where
$$u_0(x) = \frac{-8\kappa c x}{(x^2 + c^2 + 1)^2 - 4c^2 x^2} = \left(\frac{\partial \psi}{\partial y} \right)_{y=0}, \quad (\text{B } 7)$$

the tangential velocity on the free surface.

The solution is

$$\eta(x) = \frac{1}{2} \mathcal{C} \{g(x) + g(-x)\} \quad (\text{B } 8)$$

where
$$g(x) = -\kappa^{-1} \int_{-\infty}^x e^{-\beta(x-\xi)} u_0(\xi) d\xi \quad (\text{B } 9)$$

and $\beta = (\mathcal{C}G)^{1/2}$. It will be sufficient to consider two limiting cases.

(i) $\beta \ll 1$

In this limit,

$$g(x) \approx -2 \tan^{-1}(x+c) + 2 \tan^{-1}(x-c) \quad (\text{B } 10)$$

so that
$$\eta(x) = -2\mathcal{C} \{ \tan^{-1}(x+c) - \tan^{-1}(x-c) \}. \quad (\text{B } 11)$$

Figure 14 shows the free-surface shape for $c = 1$.

In the special limit of a vortex dipole ($c \rightarrow 0$, $\kappa \rightarrow \infty$ with $2c\kappa = \alpha = \text{const.}$), (B 11) gives (with $\mathcal{C} = \mu\alpha/\gamma$)

$$\eta(x) \sim \frac{-4\mathcal{C}}{x^2 + 1} \quad (\text{B } 12)$$

which agrees with the limiting form of (3.3) when $|\mathcal{C}| \ll 1$, namely

$$y \sim \frac{2a}{x^2 + 1} \sim \frac{-4\mathcal{C}}{x^2 + 1} \quad (\text{B } 13)$$

since $a \sim -2\mathcal{C}$ when $|\mathcal{C}|$ is small. Figure 14 also shows the limiting form (B 12).

(ii) $\beta \rightarrow \infty$

In this limit, (B 6) gives immediately $\eta = G^{-1} \kappa^{-1} du_0/dx$, i.e.

$$\eta = -\frac{8c(x^2 + c^2 + 1)(c^2 + 1 - 3x^2) + 4c^2 x^2}{G \{(x^2 + c^2 + 1)^2 - 4c^2 x^2\}^2}. \quad (\text{B } 14)$$

A crest is present at $x = 0$ only for $c > 1$. Figure 15 shows this form of the free surface for $c = 2$ and 0.5 and for the limiting dipole case ($c \rightarrow 0$, $2c\kappa = \alpha$) for which

$$\eta \sim -\frac{8}{G} \frac{1 - 3x^2}{(x^2 + 1)^3}, \quad (\text{B } 15)$$

with $G = \rho g/\mu\alpha$.

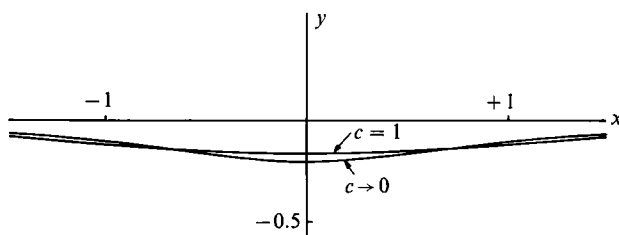


FIGURE 14. Linearized free-surface shape when $\beta \ll 1$, $\mathcal{C} = 0.05$, for $c = 1$ and for the dipole limit $c \rightarrow 0$.

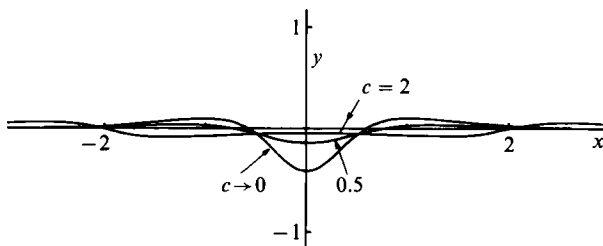


FIGURE 15. Linearized free-surface shape when $\beta \gg 1$, $G = 20$, for $c = 2, 0.5$ and for the dipole limit $c \rightarrow 0$.

Finally, note that in the dipole limit (B 7) becomes

$$u_0(x) \sim -\frac{4\alpha x}{(x^2 + 1)^2} \quad (\text{B } 16)$$

which as expected agrees with the limiting form of (3.11) as $a \rightarrow 0$.

Note added in proof. Following a seminar in DAMTP on the topic of this paper, Dr John Hinch provided the following simple and elegant explanation for the exponential dependence (3.6) of radius of curvature R on capillary number \mathcal{C} :

The surface tension exerts a force 2γ per unit length of cusp on the fluid in the cusp region. This creates a Stokes flow with stream function (1.1) and associated *upward* velocity on $x = 0$

$$u = \frac{\gamma}{2\pi\mu} \ln\left(\frac{c_1 d}{r}\right)$$

for some dimensionless constant c_1 . At a distance $\frac{1}{3}d$ from the vortex dipole (i.e. in the neighbourhood of the location where the cusp forms) there is a *downward* flow which would be $8.64\alpha/d^2$ if the free surface were flat, but is in fact increased to $c_2\alpha/d^2$ ($c_2 > 8.64$) due to the downward 'streamlining' of the free-surface shape. These two flows must balance at $r = R$ where the free surface is stationary; this balance of vertical velocity gives

$$r = c_1 d \exp\{-2c\pi\mu\alpha/d^2\gamma\} = c_1 d \exp(-2c_2\pi\mathcal{C}).$$

The exact solution shows that in fact $c_1 = \frac{256}{3}$ and $c_2 = 16$. Note that the Stokeslet singularity is at a distance R *above* the free surface (outside the fluid). The combination of Stokeslet and uniform stream gives the 'rear stagnation point' flow in the parabolic region.

REFERENCES

- BYRD, P. F. & FRIEDMAN, M. D. 1971 *Handbook of Elliptic integrals for Engineers and Scientists*, 2nd Edn. Springer.
- DUSSAN V., E. B. & DAVIS, S. H. 1974 On the motion of a fluid–fluid interface along a solid surface. *J. Fluid Mech.* **65**, 71–95.
- GRADSHTEYN, I. S. & RYZHIK, I. M. 1980 *Table of Integrals, Series and Products* (Corrected and Enlarged Edn). Academic.
- GRIGGS, D. 1939 A theory of mountain building. *Am. J. Sci.* **237**, 611–650.
- JOSEPH, D. D., NELSON, J., RENARDY, M. & RENARDY, Y. 1991 Two-dimensional cusped interfaces. *J. Fluid Mech.* **223**, 383–409.
- LISTER, J. R. 1989 Selective withdrawal from a viscous two-layer system. *J. Fluid Mech.* **198**, 231–254.
- MUSKHELISHVILI, N. I. 1953 *Some Basic Problems of the Mathematical Theory of Elasticity*, 3rd Edn. P. Noordhoff.
- RICHARDSON, S. 1968 Two-dimensional bubbles in slow viscous flows. *J. Fluid Mech.* **33**, 476–493.
- SAFFMAN, P. G. 1986 Viscous fingering in Hele-Shaw cells. *J. Fluid Mech.* **173**, 73–94.